A Computational study of Mg_mH_n nanoclusters with n:m [?] 2:1 for efficient hydrogen storage

Dongjie Shi[1], Youxuan Ni[1], Geng Li[1], Zhenhua Yan[1], Qing Zhao[1], Weiwei Xie[1], and Jun Chen[1]

[1]Institute of Applied Chemistry

June 15, 2022

Abstract

Magnesium-based hydrogen storage material (MgH_2) has attracted much attention due to its high hydrogen storage density (7.6 wt%). However, the high hydrogen dissociation enthalpy and slow hydrogen dissociation rate in bulk Mg hinder its wide application in the efficient hydrogen storage. In the present work, we study the hydrogen adsorption and desorption reactions of MgmHn (m = 1-6) nanoclusters using density functional theory (DFT). From the global search for the configurations of MgmHn nanoclusters, we found not only stable saturated MgmHn (n = 2m) nanoclusters, but four hydrogen-enriched MgmHn (n:m>2:1) nanoclusters, Mg3H7, Mg4H9, Mg5H11, Mg6H13, with the hydrogen storage density higher than 8.3 wt%. The electronic-structure calculations indicate that the stability of the hydrogen-enriched cluster gets relatively higher for larger nanocluster. The *ab initio* dynamics simulations shows that all hydrogen-enriched clusters have very fast hydrogen dissociation rates, which is promising for the hydrogen dissociation at ambient temperature and pressure. This work provides insights into the hydrogen storage mechanism of nano-magnesium materials.

A Computational study of Mg_mH_nnanoclusters with n:m [?] 2:1 for efficient hydrogen storage

Dongjie Shi 11*Renewable Energy Conversion and Storage Center (RECAST), Haihe Laboratory of Sustainable Chemical Transformations, Key Laboratory of Advanced Energy Materials Chemistry (Ministry of Education), College of Chemistry, Nankai University, Tianjin, 300071, China.* **, Youxuan Ni [1], Geng Li [1],** 22*National Supercomputer Center in Tianjin, Tianjin 300457, China* **, Zhenhua Yan[1], Qing Zhao [1],Weiwei Xie[1], *, Jun Chen [1]**

Correspondence to: *Weiwei Xie, Key Laboratory of Advanced Energy Materials Chemistry (Ministry of Education), College of Chemistry, Nankai University, Tianjin, 300071, China.*

E-mail:*xieweiwei@nankai.edu.cn*

Introduction

Hydrogen is the fuel with high energy density and clean resource, which may be a promising energy carrier to replace hydrocarbons. However, the difficulty in the efficient storage of hydrogen is considered to be a key challenge in the application of hydrogen resource [1, 2]. One of the most viable and effective possible solutions is to store hydrogen in metal hydrides [3-5]. Among lightweight chemical hydrides, magnesium hydride (MgH_2) has been widely studied due to its low cost and high hydrogen capacity of up to 7.6 wt%. However, bulk MgH_2 has high desorption energy (75 kJ/mol) and sluggish reaction kinetics, leading to a high temperature (573 K) for hydrogen release [6, 7]. Considerable approaches have been conducted on improving the thermodynamics and kinetics of MgH_2, such as additive-addition (adding metal oxides, metal halides, or carbon adding etc.) [8, 9] and alloying [10, 11]. Although these approaches can effectively reduce the operating temperature, the additional weight of additive leads to a lower hydrogen storage capacity in

comparison to the bulk MgH_2 [12, 13]. Recently, nanosizing magnesium-based hydrides have been proposed as an alternative method for improving hydrogen storage capacity [14, 15]. Since the large specific surface area of nanostructure increases the ability of hydrogen adsorption, the Mg nanoparticles have superior hydrogen storage property in comparison with bulk Mg [16-18]. Moreover, the large specific surface area can shorten the diffusion path of adsorbed hydrogen atoms, accelerating hydrogen release.

Many experiments and theoretical calculations have confirmed that nanosizing Mg particles can effectively improve the hydrogen storage properties of MgH_2 [4, 16, 19-21]. Xia et al. synthesized monodisperse MgH_2 nanoparticles with an average size of 4.7-6.0 nm under the structure-directing role of graphene. These MgH_2 nanoparticles could release 5.4 wt% hydrogen at 250°C within 30 min and the formation enthalpy of MgH_2 is reduced to 62.1 kJ/mol, in comparison to 75 kJ/mol for bulk MgH_2 [22]. Zhang et al. developed ultrafine MgH_2 hydrides of 4-5 nm without involving any scaffold or protection agent. The hydrogen release enthalpy is decreased to 59.5 kJ/mol [23]. Konarova M. et al. loaded MgH_2into CMK3 mesoporous scaffolds with a pore size of only 3.5 nm. The dissociation enthalpy of the MgH_2/CMK3 composite is 52.38 kJ/mol H_2, and the initial dissociation temperature 253°C, which is much lower than the bulk MgH_2 (300-400°C) [24].

Theoretically, Li et al. have performed the DFT calculations for the effect of size of nanowires on the thermodynamic stability of MgH_2 nanowires. They found the desorption enthalpies of φ0.85 nm ($MgH_{2.33}$) and φ1.24 nm ($MgH_{2.17}$) nanowires are reduced to 34.54 kJ/mol and 68.22 kJ/mol [25-27] respectively. Although Mg-H nanowires improve hydrogen storage capacity, the structures are unstable and will collapse into nanoparticles after a few cycles [21]. For nanoclusters, the first-principle calculation by Wagemans et al. showed that the hydrogen desorption enthalpy of Mg_9H_{18} cluster is 63 kJ/mol, corresponding to the hydrogen release temperature of 200 [28]. H. Chen et al. carried out the density functional theory (DFT) calculations for hydrogen dissociation reactions of MgH_2nanoclusters doped by a Sc atom, and found that $MgScH_{15}$cluster has a high hydrogen storage capacity of 17.8 wt% [29]. Aditya Kumar et al. found Mg_2B_6 cluster has a maximum H_2 adsorption of 8.10 wt% at ambient temperature and 1 bar pressure [30]. Although the first-principle calculations show that the doped elements can improve the hydrogen storage capacity, the high weight and cost of dopant limit its application in hydrogen storage using magnesium hydride.

While many works have focused on the thermodynamics and kinetics of saturated Mg_mH_n (n = 2m) nanoclusters, to our best knowledge, no literature reports the Mg_mH_n nanoclusters with the stoichiometric composition of n:m > 2. In the present study, we find four hydrogen-enriched Mg_mH_n (n:m>2:1) nanoclusters, Mg_3H_7, Mg_4H_9, Mg_5H_{11}, Mg_6H_{13}, in which the hydrogen capacities are higher than 8.3 wt%. The *ab initio* molecular dynamics simulations show that the hydrogen dissociation reactions of hydrogen-enriched nanoclusters occur at a very short time (< 200fs) at room temperature, which may be promising for the hydrogen release at ambient temperature and pressure. This work deepens the understanding of the kinetic mechanism of hydrogen dissociation reaction for Mg_mH_n (n[?]2m) and provides new insights into the hydrogen storage of nano-magnesium materials.

Methods

To determine the reliable and accurate computational method, we examined the performance of a variety of computational methods, including B3LYP-D3, ωB97XD, M062X and MP2, in the calculations of the bond lengths, frequencies, and binding energies of MgH, H_2, and Mg_2. The comparison with experimental results [31, 32] is shown in Table 1. The bond lengths of MgH, H_2 and Mg_2 calculated by B3LYP-D3, ωB97XD and M062X functionals are in good agreements with experimental values, while the MP2 method strongly overestimates the bond lengths of Mg_2. The B3LYP-D3 overestimates the stretching frequency of Mg_2. For the binding energies of MgH, M062X reproduces the experimental value quite well, while ωB97XD gives a higher binding energy. Since M062X functional provides a good description of the Mg-Mg and Mg-H bonding interaction, it will be used in the study of hydrogen desorption reactions of Mg_mH_n clusters.

Initially, 400 configurations of Mg_mH_n(m = 1-6) nanoclusters with the hydrogen-hydrogen distance less than 1.0 were generated from 3000 configurations sampled using Molclus program [33]. These structures were used as initial structures for the geometry optimization using M062X/6-311G (d, p) method implemented

in Gaussian 16 [34]. For each type of Mg_mH_n cluster, the structure with minimum electronic energy was employed for the geometry optimization using a higher level of M062X/def2TZVP. Frequency calculations were performed to determine the local minimum in potential energy surfaces. The electron localized function (ELF) were calculated using Multiwfn 3.9 program [35]. The *ab initio* molecular dynamics (AIMD) simulations for the hydrogen dissociation reactions of Mg_mH_n (n [?] 2m) nanoclusters were carried out using M062X/def2TZVP method implemented in ORCA program [36]. The simulation time was 5000 fs with a time step of 1.0 fs. The Berendsen thermostat [37] was used to obtain a correct canonical ensemble at 300K.

Table 1. Comparison of calculated bond lengths, frequencies, and binding energies of MgH, H_2, Mg_2 with experiments.

	MgH	H_2	Mg_2
Bond lengths / Å	1.749[a]	0.744[a]	3.917[a]
	1.744[b]	0.744[b]	3.929[b]
	1.731[c]	0.741[c]	3.820[c]
	1.731[d]	0.738[d]	4.396[d]
	1.730[e]	0.741[e]	3.890[e]
Frequencies / cm^{-1}	1433.42[a]	4419.20[a a]	133.26[a]
	1471.74[b]	4435.12[b]	50.41[b]
	1551.61[c]	4472.73[c]	70.60[c]
	1551.61[d]	4533.23[d]	28.28[d]
	1495.20[e]	4401.21[e]	45.00[e]
Binding Energies / eV	1.43[a]	4.77[a]	0.18[a]
	1.41[b]	4.65[b]	0.05[b]
	1.32[c]	4.68[c]	0.06[c]
	1.26[d]	4.37[d]	0.02[d]
	1.31[e]	4.52[e]	0.05[e]
a. B3LYP-D3/6-311G(d, p); b. ωB97XD/6-311G(d, p); c. M062X/6-311G(d, p); d. MP2/6-311G(d, p); e. Experiments [31, 32]	a. B3LYP-D3/6-311G(d, p); b. ωB97XD/6-311G(d, p); c. M062X/6-311G(d, p); d. MP2/6-311G(d, p); e. Experiments [31, 32]	a. B3LYP-D3/6-311G(d, p); b. ωB97XD/6-311G(d, p); c. M062X/6-311G(d, p); d. MP2/6-311G(d, p); e. Experiments [31, 32]	a. B3LYP-D3/6-311G(d, p); b. ωB97XD/6-311G(d, p); c. M062X/6-311G(d, p); d. MP2/6-311G(d, p); e. Experiments [31, 32]

The adsorption energy of Mg_mH_n is defined by taking H_2 and Mg_m clusters as references,

$E_a(Mg_mH_n) = E(Mg_mH_n) - E(Mg_m) - n/2\ E(H_2)$ (1)

where $E(Mg_mH_n)$, $E(Mg_m)$ represent the energy of Mg_mH_n, Mg_m clusters, respectively. $E(H_2)$ is the energy of H_2 molecule.

For hydrogen desorption reaction, the average desorption energy per H_2 mole of Mg_mH_n cluster is given by

$<E_d(Mg_mH_n)> = [E(Mg_m) + n/2\ E(H_2) - E(Mg_mH_n)]/n$ (2)

The stepwise desorption energy ([?]E_d) for Mg_mH_n cluster is described in relation to the energy of Mg_mH_{n-2} of the previous step ($E(Mg_mH_{n-2})$),

$[?]E_d(Mg_mH_n) = E(Mg_mH_{n-2}) + E(H_2) - E(Mg_mH_n)$ (3)

Note that the zero-point energy correction (ZPE) has been included in the calculation of adsorption energy, average desorption and stepwise desorption energies.

At each step of the hydrogen desorption reactions of Mg_mH_n (n = 2m) clusters, the pair of hydrogen atoms with lowest dissociation barrier is detached from the cluster. To compute transition state (TS), we first performed relaxed potential energy scan using M062X/6-31G(d) method for the hydrogen pairs with the pair distance less than 4.0 Å. Only the hydrogen pair distance was kept constant while all other degrees of freedom were relaxed. The hydrogen pair distance was reduced with a step of 0.1 Å until the distance is less than 1 Å. The structure with highest energy was used as the initial guess for the TS optimization at a high level of M062X/def2TZVP. The frequency analysis was performed to determine the saddle point of potential energy surface.

Results and discussion

3.1 Mg_mH_n Cluster Structures

Figure 1 displays the structures of Mg_mH_n (m = 1-6, n [?] 2m) clusters obtained from the global configuration search. It can be seen that the skeleton of Mg_m cluster is dramatically reconstructed as more hydrogen atoms are added. Most hydrogen atoms locate in bridging positions between two or more Mg atoms. The saturated Mg_3H_6, Mg_4H_8, Mg_5H_{10}, Mg_6H_{12} clusters are identical to the structures reported in a recent study by Emmanuel [4], which confirms the accuracy of the global search method. In addition to saturate structures, the oversaturated Mg_3H_7, Mg_4H_9, Mg_5H_{11}, Mg_6H_{13} (stoichiometric composition of Mg:H > 1:2) clusters are found from the global search. These hydrogen-enriched structures may be the intermediates in hydrogen adsorption/desorption reaction. Note that the structures of Mg_mH_n (n > 2m) obtained by geometry optimization using other functionals (B3PW91, HSE06 and PBE0) are identical with M062X structures. Adding more hydrogen atom leads to the decomposition of the nanoclusters (Mg_3H_8, Mg_4H_{10}, Mg_5H_{12}, Mg_6H_{14}) into a hydrogen molecule and Mg_mH_{2m} clusters.

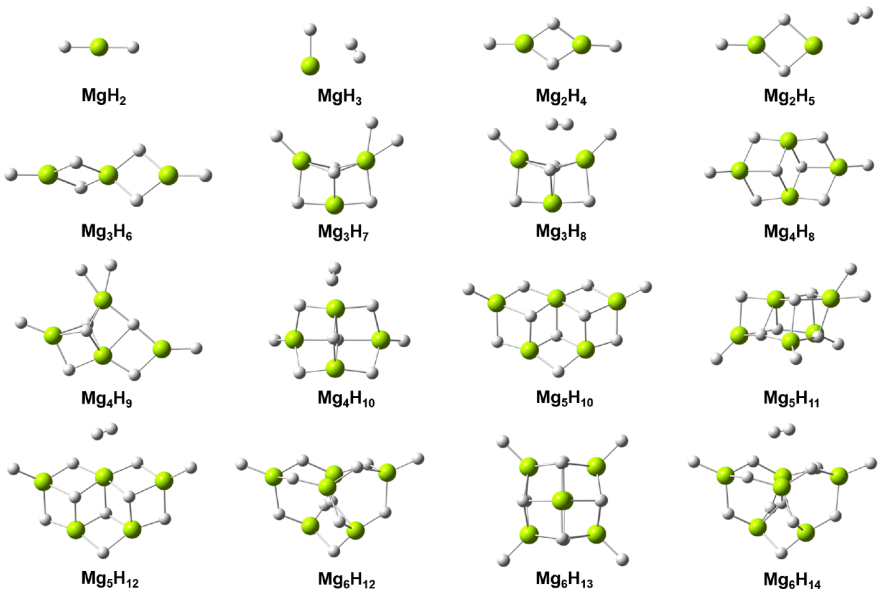

Figure 1. Lowest-energy structures of Mg_mH_n(n [?] 2m) clusters calculated at M062X/def2TZVP level. The green and white balls represent Mg and H atoms, respectively.

3.2 Hydrogen Adsorption of Mg_mH_nClusters

The adsorption energies (E_a) of Mg_mH_n (m = 3-6, n = 1-13) clusters are shown in Figure 2a. The adsorption energy of these structures was further verified with CCSD (T)/def2TZVP and shown in Table S1 in Supporting Information. Thermodynamically, the lower is the adsorption energy, the more stable the structure is. For Mg_mH_n (n < 2m), as the number of adsorbed hydrogen atoms increases, the adsorption energies of the

clusters tend to be more negative until Mg:H = 1:2. The clusters with the stoichiometric ratio of Mg:H of 1:2 are the most stable. When the hydrogen atoms are further adsorbed, the adsorption energy of oversaturated Mg_mH_n (n = 2m+1) structures rises significantly, which indicates that Mg_mH_n (n = 2m+1) are less stable than saturated Mg_mH_n (n = 2m). However, it is noted that the hydrogen adsorption reaction in reality usually occurs under the high-pressure condition [38, 39], in which the hydrogen-enriched clusters can exist. As shown in Figure 2b, as the size of Mg_m clusters increases, the adsorption energy of Mg_mH_n (n = 2m+1) gradually decreases and the structure becomes relatively more stable. The adsorption energies of Mg_3H_7, Mg_4H_9 are all above zero, while for Mg_5H_{11}, Mg_6H_{13}, the adsorption energies are negative. These indicate that the formation of Mg_3H_7, Mg_4H_9 is endothermic reaction while the formation of Mg_5H_{11}, Mg_6H_{13} is exothermic reaction.

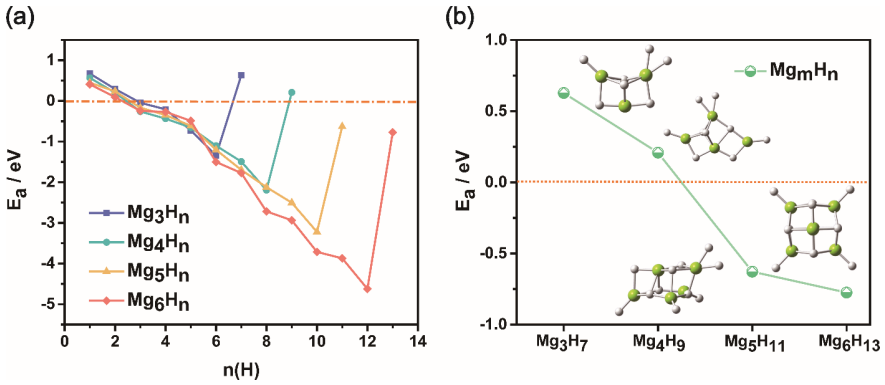

Figure 2. (a) Adsorption energy of Mg_mH_n(m=3-6, n=1-13) and (b) hydrogen-enriched nanoclusters.

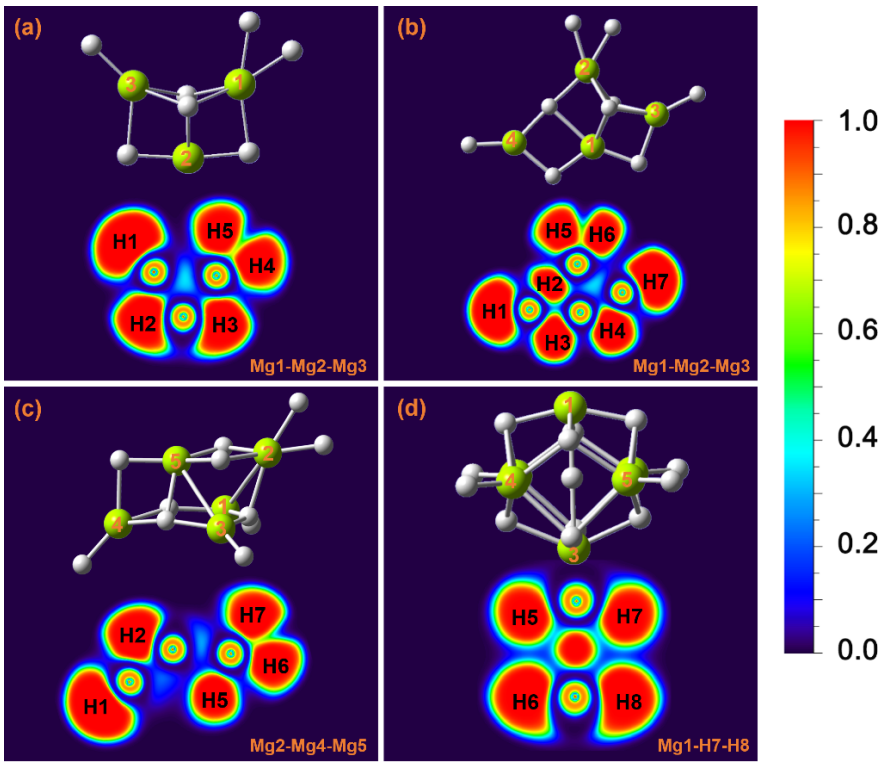

Figure 3. Two-dimensional ELF of (a) Mg_3H_7 (b) Mg_4H_9 (c) Mg_5H_{11}, and (d) Mg_6H_{13} clusters. Green and white balls stand for Mg and H atoms, respectively. The projection plane is determined by the three Mg atoms marked with labels shown at the bottom of the panels.

To gain further insights into the stability of oversaturated Mg_mH_n (m = 3-6, n = 2m+1) clusters, we perform the electronic-structure analysis for Mg_3H_7, Mg_4H_9, Mg_5H_{11} and Mg_6H_{13} clusters using electron localized function (ELF) [40]. Figure 3 shows the comparison of the two-dimensional (2D) ELF projection diagrams of Mg_3H_7,Mg_4H_9,Mg_5H_{11}, and Mg_6H_{13} clusters, where the projection plane is determined by the three Mg atoms marked at the bottom of each panel. The high ELF value indicates a strong electronic localization. It can be seen that the electrons around hydrogen atoms are strongly localized for all clusters. The minimum ELF value between Mg and H indicates an ionic character of Mg-H bond. For the Mg_3H_7 cluster, ELF values between H4 and H5 atoms are around 0.6 (Figure 3a), indicating a covalent interaction between H4 and H5 atoms. This covalent interaction is also found in the hydrogen pairs of H5-H6 in Mg_4H_9 cluster and of H6-H7 in Mg_5H_{11} cluster (Figure 3b and 3c). However, the ELF value between hydrogen atoms (H5-H6 and H7-H8) in Mg_6H_{13} cluster is much smaller (about 0.2) (Figure 3d), which indicates a relatively weaker covalent interaction and higher stability of Mg_6H_{13} cluster.

3.2 Hydrogen Dissociation of Mg_mH_nClusters

To explore hydrogen dissociation of the saturated Mg_mH_{2m} and hydrogen-enriched Mg_mH_{2m+1} clusters, we carried out AIMD simulations at room temperature for 5ps. The potential energies for saturated and hydrogen-enriched clusters are shown in Figure 4a and Figure 4b, respectively. It can be seen that the time-dependent potential energies for saturated Mg_mH_{2m} clusters fluctuate near the equilibrium energy, which indicates the clusters are quite stable during the simulation time. In contrast, the time-dependent potential energy the hydrogen-enriched nanoclusters Mg_mH_{2m+1} show a very fast energy decreasing within 200fs, which indicates the hydrogen dissociation reactions occurs at a very short time scale. This can be also demonstrated in the time-dependent H-H distance shown in Figure 4(c)-(d). For the saturated clusters (Figure 4(c)), the H-H distance only oscillates around ˜ 3.2 during 5 ps simulation, while the hydrogen molecule is generated within 200 fs. Somehow unexpectedly, Mg_6H_{13} with more negative adsorption energy (Figure 2b) have the faster hydrogen dissociation reaction rate than Mg_4H_9 and Mg_5H_{11} clusters. The underlying reason is still not clear and needs further investigation.

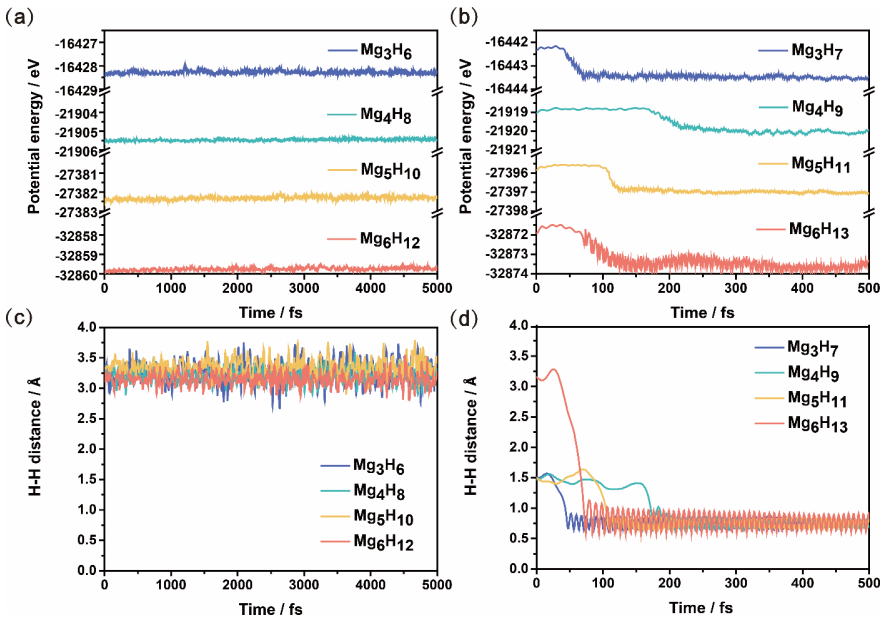

Figure 4. Time evolution of the potential energies and representative hydrogen-hydrogen pair distance of (a), (c) Mg_mH_{2m} and (b), (d) Mg_mH_{2m+1} clusters at 300K.

As discussed above, the hydrogen dissociation reactions for saturated Mg_mH_{2m} clusters were not observed in our AIMD simulations. To further understand hydrogen dissociation reactions of the saturated Mg_mH_{2m} clusters, we perform hydrogen desorption energies and barrier heights of hydrogen dissociation reactions of the saturated Mg_mH_{2m} clusters. Fig. 5a shows the average desorption energy ($<E_d>$) as a function of cluster size. Overall, the average desorption energy increases monotonically for larger size of clusters and approaches the experimental value of 0.81 eV for bulk MgH_2. The inclusion of ZPE slightly shifts down the average desorption energy for larger clusters. Figure 5b shows the stepwise desorption energies ([?]E_d) of Mg_mH_n (m = 3-6) clusters. From m=4 to 6, the stepwise desorption energy first rises slightly and then decreases abruptly with the lower content of hydrogen in the clusters. This indicates that less and less energy is needed for the dissociation of hydrogen molecule as the desorption reaction proceeds. Interestingly, the production of the last $H_2$is exothermic reaction, in consistent with endothermic reaction for the adsorption of the first H_2 in the clusters.

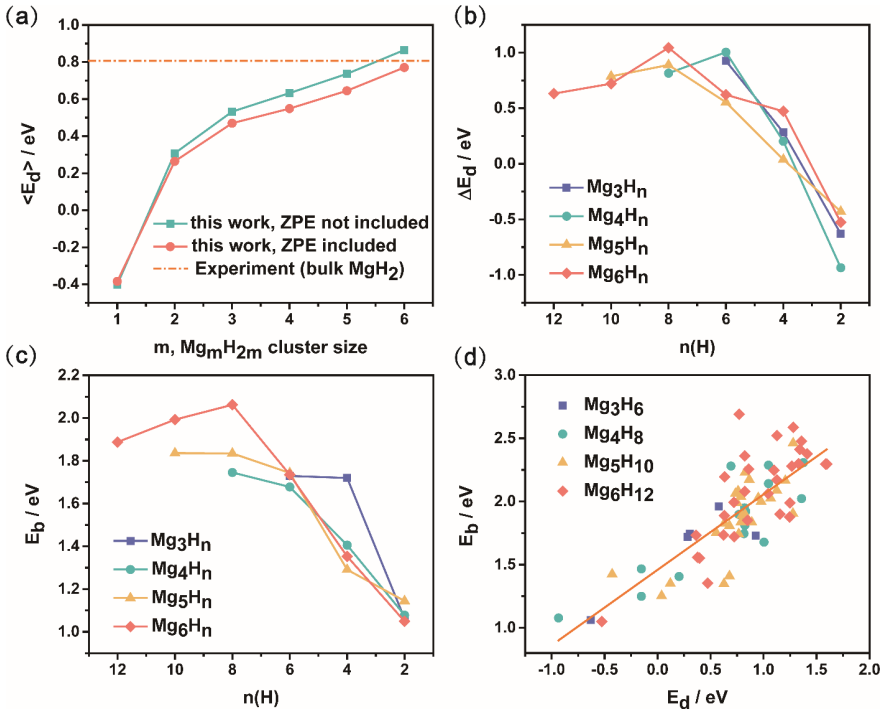

Figure 5. (a) Average desorption energy ($<E_d>$) calculated with/without ZPE as a function of cluster size, (b) Stepwise desorption energy (ΔE_d) and (c) activation barrier (E_b) for Mg_mH_{2m} (m = 3-6) clusters, (d) Relation between stepwise desorption energy and activation barrier of Mg_mH_{2m} (m = 3-6) clusters.

To understand the kinetic properties of desorption reaction, we calculate the barrier height (E_b) for each step of desorption reaction of Mg_mH_{2m} (m = 3-6) clusters and the reaction profiles are shown in Figure. S1 (Supporting information). Figure 5c shows the activation barrier as a function of number of hydrogen atoms in the clusters. For Mg_6H_n, the activation barrier first rises from 1.88 eV to 2.06 eV, and then decrease dramatically for n<8. For Mg_5H_n (n=8-4), Mg_4H_n and Mg_3H_n, the dissociation barrier tends to be lower as the number of the adsorbed hydrogen atoms decreases, which indicates that the hydrogen desorption reaction become more favorable. This trend is similar to the change of the stepwise desorption energy with the lower hydrogen content in the clusters. Figure 5d shows the relation between the stepwise desorption energy and the dissociation barrier. The scatter points are fitted with a linear function with the slope of

1.459, intercept of -0.409 eV and mean absolute error (MAE) of 0.20 eV. The linear energy relation is so-called Brønsted–Evans–Polanyi (BEP) relation, which describes the linear correlations between transition states and reactions energies.

Conclusions

In the present work, we study the thermodynamics as well as kinetics of the hydrogen adsorption and desorption reactions of Mg_mH_n clusters (m=1-6, n[?]2m) using M062X/def2TZVP method. The saturated stable Mg_mH_{2m} and oversaturated Mg_mH_{2m+1} clusters: Mg_3H_7, Mg_4H_9, Mg_5H_{11}, Mg_6H_{13} with the hydrogen storage density higher than 8.3 wt% are found in the global search of the stable configurations. It is found that the larger size of cluster, the higher stability of oversaturated cluster. Although they are less stable than the saturated Mg_mH_{2m} (m = 3-6) clusters, experimentally, we expect they can exist under the high pressure. The AIMD simulations show that the hydrogen dissociation reaction of hydrogen-enriched Mg_mH_{2m+1} clusters occurs at a very fast time scale (< 200 fs). These materials may be promising for hydrogen release at ambient temperature and pressure. Next, we investigate the kinetic properties of the saturated Mg_mH_{2m} clusters. Both stepwise desorption energies and barrier heights decrease as the hydrogen content in the clusters decreases, indicating that the hydrogen desorption reaction become more favorable as the reaction proceeds. Moreover, the linear correlation between the stepwise desorption energy and activation barrier indicates that BEP relation holds in the hydrogen desorption reactions of Mg_mH_{2m} clusters. This work provide new insights into the mechanisms of efficient hydrogen storage using magnesium-based nanomaterials.

Acknowledgments

This study was supported by National Key R&D Program of China (2018YFB1502101), National Natural Science Foundation of China (22121005, 22005155, 52072186, 52001170, and 52001171). The calculations were carried out at National Supercomputer Center in Tianjin by TianHe-1A.

Declaration of competing interest

All authors approved this submission and there are no conflicts to declare. We confirm that this work is original and has not been published, and is not being submitted to any other journals during this submission.

References

[1] Schapbach, Louis, Zuttel, Andreas, *Nature* . **2001** , 414, 353-353.

[2] T. He, P. Pachfule, H. Wu, Q. Xu, P. Chen, *Nat. Rev. Mater.* **2016** , 1, 1-17.

[3] L. Li, Y. Huang, C. An, Y. Wang, *Sci. China Mater.***2019,** 62, 1597-1625.

[4] E. N. Koukaras, A.D. Zdetsis, M. M. Sigalas, *J. Am. Chem. Soc.* **2012** , 134, 15914-15922.

[5] T. Wang, X. Cao, L. Jiao,*eScience.* **2021,** 1, 69-74.

[6] J. C. Crivello, B. Dam, R.V. Denys, M. Dornheim, D.M. Grant, J. Huot, T. R. Jensen, P. de Jongh, M. Latroche, C. Milanese, D. Milčius, G. S. Walker, C. J. Webb, C. Zlotea, V. A. Yartys,*Appl. Phys. A.* **2016,**122, 1-20.

[7] F. Cheng, Z. Tao, L.J. Chen, *ChemComm.* **2012** , 48, p.7334-7343.

[8] X. Zhang, K. Wang, X. Zhang, J. Hu, Y. Liu, *Int. J. Energy Res.* **2021,** 45, 3129-3141.

[9] X. Lu, L. Zhang, H. Yu, Z. Lu, J. He, J. Zheng, F. Wu, L. Chen,*Chem. Eng. J.* **2021** , 422, 130101.

[10] V. Berezovets, R. Denys, I. Y. Zavaliy, Y. V. Kosarchyn,*Int. J. Hydrog. Energy.* **2021,** 47,7289-7298.

[11] Y. Liu, Y. Cao, H. Pan, *J. Alloys Compd.* **2011,**509, 675-686.

[12] Y. Wang, Y. Wang, *Prog. Nat. Sci.* **2017,** 27, 41-49.

[13] L. Ouyang, F. Liu, H. Wang, J. Liu, X.-S. Yang, L. Sun, M. Zhu,*J. Alloys Compd.* **2020,** 832, 154865.

[14] N.S. Norberg, T.S. Arthur, S. J. Fredrick, A. L. Prieto,*J. Am. Chem. Soc.* **2011,** 133, 10679.

[15] P. Vajeeston, P. Ravindran, M. Fichtner, H. Fjellvag, *J. Phys. Chem. C* . **2012** , 116, 18965-18972.

[16] S.A. Shevlin, Z.X. Guo, *J. Phys. Chem. C.* **2013,**117, 10883-10891.

[17] Z. Wu, M.D. Allendorf, J.C. Grossman, *J. Am. Chem. Soc.***2009** , 131, 13918-13919.

[18] M. K. Singh, A. Bhatnagar, S. K. Pandey, P. Mishra, O. Srivastava, *Int. J. Hydrog. Energy.* **2017,** 42, 960-968.

[19] K. Iyakutti, V. Surya, R. Lavanya, V. Vasu, R. Rajeswarapalanichamy, Y. Kawazoe, *Comput. Condens. Matter.***2022,** e00643.

[20] D. Shen, C.P. Kong, R. Jia, P. Fu, H. X. Zhang, *J. Phys. Chem. A* . **2015,** 119, 3636-3643.

[21] T. Sadhasivam, H.-T. Kim, S. Jung, S.-H. Roh, J.-H. Park, H.-Y. Jung, *Renew. Sust. Energ. Rev.* **2017,** 72, 523-534.

[22] G. Xia, Y. Tan, X. Chen, D. Sun, Z. Guo, H. Liu, L. Ouyang, M. Zhu, X. Yu, *Adv. Mater.* **2015,** 27, 5981-5988.

[23] X. Zhang, Y. Liu, Z. Ren, X. Zhang, J. Hu, Z. Huang, Y. Lu, M. Gao, H. Pan, *Energy Environ. Sci.* **2021** , 14, 2302-2313.

[24] M. Konarova, A. Tanksale, J. N. Beltramini, G. Q. Lu,*Nano Energy* . **2013,** 2, 98-104.

[25] B. Peng, L. Li, W. Ji, F. Cheng, J. Chen, *J. Alloys Compd.* **2009,** 484, 308-313.

[26] W. Li, C. Li, H. Ma, J. Chen, *J. Am. Chem. Soc.***2007** ,129, 6710-6711.

[27] L. Li, B.Peng, W. Ji, J. Chen, *J. Phys. Chem. C* .**2009,** 113, 3007-3013.

[28] R. W. P. Wagemans, J. H. van Lenthe, P. E. de Jongh, A. J. van Dillen, K. P. de Jong, *J. Am. Chem. Soc.* **2005,** 127, 16675-16680.

[29] H. Chen, H. Liang, W. Dai, C. Lu, K. Ding, J. Bi, B. Zhu,*Int. J. Hydrog. Energy.* **2020,** 45, 32260-32268.

[30] A. Kumar, N. Vyas, A.K. Ojha, *Int. J. Hydrog. Energy.***2020,** 45, 12961-12971.

[31] F. Ruette, M. Sánchez, R. Añez, A. Bermúdez, A. Sierraalta,*J. Mol. Struct.:Theochem* 2005, 729, 19-37.

[32] W. Balfour, A. Douglas, *Can. J. Phys.* **1970,** 48, 901-914.

[33] T. Lu, Molclus program. Version 1.9, http://www.keinsci.com/ research/molclus.html.

[34] M. Frisch, G. Trucks, H. Schlegel, G. Scuseria, M. Robb, J. Cheeseman, G. Scalmani, V. Barone, G. Petersson, H. Nakatsuji, Gaussian, Inc. Wallingford, CT, 2016.

[35] T. Lu, F. Chen, *J. Comput. Chem.* **2012,** 33, 580-592.

[36] F. Neese, *Rev: Comput. Mol. Sci.* **2012,** 2, 73-78.

[37] T. Straatsma, H. Berendsen, J. Postma, *J. Chem. Phys* .**1986** , 85, 6720-6727.

[38] D. C. Lonie, J. Hooper, B. Altintas, E. Zurek, *Phys. Rev. B* . **2013,** 87, 054107.

[39] X. Feng, J. Zhang, G. Gao, H. Liu, H. Wang, *RSC Adv.***2015,** 5, 59292-59296.

[40] W. Zhang, Y. Zhang, Y. Li, S. Yang, L.-H. Zhang, F. Yu,*Chem. Eng. Sci.* **2021,** 236.